

1 **Mechanical characterisation of the developing cell wall layers of tension wood**
2 **fibres by Atomic Force Microscopy**

3 O. Arnould¹, M. Capron^{1a}, M. Ramonda², F. Laurans³, T. Alméras¹, G. Pilate³, B. Clair¹

4
5 Running title: Mechanical properties of developing secondary wall by AFM

6 ¹ LMGC, Univ. Montpellier, CNRS, Montpellier, France

7 ² CTM, Univ. Montpellier, Montpellier, France

8 ³ INRAE, ONF, BioForA, Orléans, France

9 olivier.arnould@umontpellier.fr

10 Date of submission:

11 Number of tables: 1

12 Number of figures: (colour in print) 9

13 Word count (start of the introduction to the end of the acknowledgements, excluding materials and
14 methods): 5656

15 Supplementary data number of figures, tables or videos: 3 figures

^a Now at: Partnership for Soft Condensed Matter PSCM, ESRF The European Synchrotron Radiation Facility, Grenoble, France

16 **Highlight**

17 New insights into the changes in mechanical properties within the cell wall of poplar tension wood
18 fibres during maturation have been obtained using atomic force microscopy.

19

20 **Abstract**

21 Trees can generate large mechanical stresses at the stem periphery to control the orientation of their
22 axes. This key factor in the biomechanical design of trees, named “maturation stress”, occurs in wood
23 fibres during cellular maturation when their secondary cell wall thickens. In this study, the spatial
24 and temporal stiffening kinetics of the different cell wall layers were recorded during fibre maturation
25 on a sample of poplar tension wood using atomic force microscopy. The thickening of the different
26 layers was also recorded. The stiffening of the CML, S₁ and S₂-layers was initially synchronous with
27 the thickening of the S₂ layer and continued a little after the S₂-layer reached its final thickness as the
28 G-layer begins to develop. In contrast, the global stiffness of the G-layer, which initially increased
29 with its thickening, was almost stable long before it reached its final maximum thickness. A limited
30 radial gradient of stiffness was observed in the G-layer, but it decreased sharply on the lumen side,
31 where the new sub-layers are deposited during cell wall thickening. Although very similar at the
32 ultrastructural and biochemical levels, the stiffening kinetics of the poplar G-layer appears to be very
33 different from that described in maturing bast fibres.

34

35 **Keywords**

36 Atomic Force Microscopy; Cell wall; G-layer; Indentation modulus; Maturation; Poplar; Stiffening;
37 Tension wood; Thickening.

38

39 **Abbreviations**

40 AFM: Atomic force microscopy

41 PF-QNM: Peak-force quantitative nano-mechanics

42 MFA: Microfibril angle

43

44 Introduction

45 Wood fibres have mechanical functions in the living tree. Mature wood fibres give the tree axis
46 sufficient stiffness and strength to withstand its own weight and additional loads such as wind or
47 fruits (Niklas, 1992). In addition to this “skeletal” function, wood fibres also have a “muscular”
48 function to control the posture of the tree by actively generating forces that can bend the stem upwards
49 or compensate for the effect of gravity (Alméras and Fournier, 2009; Alméras *et al.*, 2018; Fournier
50 *et al.*, 2014; Moulia *et al.*, 2006; Scurfield, 1973). During their maturation, wood fibre cell walls
51 undergo significant physico-chemical changes that would result in major deformation if they were
52 not prevented by the older, stiff tissue, surrounding them. In place of strain, this leads to the
53 development of a high mechanical stress named “maturation stress”. Maturation stress is particularly
54 high in reaction wood (Archer 1986), a specialised tissue produced by the tree in response to
55 mechanical disturbance. In angiosperms, reaction wood is called tension wood because its maturation
56 stress tension is high, of the order of several tens of MPa. Tension wood acts like muscle by pulling
57 on one side of the stem, thereby enabling its reorientation (Okuyama *et al.*, 1994; Yamamoto, 1998).
58 Mechanical stress is known to be generated in a specific cell wall layer of tension wood fibres, named
59 the G-layer (Côté *et al.*, 1969; Dadswell and Wardrop, 1955; Fang *et al.*, 2008; Ghislain and Clair,
60 2017; Onaka, 1949). However, the mechanisms responsible for the generation of high tensile stress
61 during G-layer maturation are still the subject of debate. Several hypothetical models have been
62 proposed, which are reviewed in Alméras and Clair (2016). Gaining knowledge on the chemical,
63 physical and mechanical states of the material and their changes during cell wall maturation have
64 proven particularly useful in distinguishing between these models. For example, it has been observed
65 that the G-layer contains mesopores of several nanometres (Chang *et al.*, 2009; Clair *et al.*, 2008),
66 and that these pores swell during maturation (Chang *et al.*, 2015). It has also been shown that
67 crystalline microfibrils are under tension during maturation (Clair *et al.*, 2011). The synchronicity
68 between these two phenomena supports the hypothesis that pore swelling is related to the induction
69 of maturation stresses in the G-layer (Alméras and Clair, 2016).

70

71 A crucial factor is the change in cell wall stiffness during maturation. Indeed, using mechanical
72 modelling, it has been shown that the relative kinetics of stiffening and stress induction affect the
73 resulting state of stress in the tree (Alméras *et al.*, 2005; Pot *et al.*, 2014; Thibaut *et al.*, 2001). As
74 reported by Thibaut *et al.* (2001), the tendency of the material to deform in response to physico-
75 chemical changes can result in stress of high magnitude only if the cell wall is already sufficiently
76 stiff. To the best of our knowledge, information on the stiffening dynamics of (tension) wood cell
77 wall layers is currently lacking and the only measurements available are at the tissue scale (Grozdzits
78 and Ifju, 1969; Pot *et al.*, 2013a; 2013b).

79 One of the most promising and frequently used techniques today, nanoindentation, probes the
80 mechanical properties at the cell wall scale. It enables access to the mechanical properties within the
81 cell wall layers with modifications reduced to a minimum. This technique has already been used to
82 estimate the indentation modulus of mature native or thermo-mechanically modified cell walls of
83 wood fibres (Eder *et al.*, 2013), lignifying spruce tracheid secondary cell walls (Gindl *et al.*, 2002)
84 and (thick) fibre cell walls within a maturing vascular bundle of bamboo (Wang *et al.*, 2012; Huang
85 *et al.*, 2016). However, as widely recognized in the case of metal materials, the radius of the
86 plastically affected volume around the indenter is about three times the residual indent size for an
87 isotropic material and even more for the elastically affected one (Johnson 1987; Sudharshan Phania
88 and Oliver, 2019). This technique therefore requires a layer thickness at least three times the size of
89 the indent, which are typically in the micrometre range, to avoid measurement artefacts (Jakes *et al.*,
90 2009). As the width of the cell wall layers in the developing and maturation stages vary from almost
91 zero (cambium, beginning of the layer deposition) to a few micrometres (mature S₂ and/or G-layer),
92 interpreting the measurements obtained by nanoindentation in the presence of a gradient of properties
93 or within a thin layer is not straightforward, nor possible close to the cambium, due to boundary
94 effects. In such cases, atomic force microscopy (AFM) appears to be the best way to perform
95 mechanical measurements within each cell wall layer (Arnould and Arinero, 2015; Casdorff *et al.*,
96 2017; 2018; Clair *et al.*, 2003, Coste *et al.*, 2021; Nair *et al.*, 2010; Normand *et al.*, 2021). This
97 technique has already been used to investigate, for example, the development of bast fibres within a
98 flax stem (Goudenhoofft *et al.*, 2018) and of the primary cell walls in the inner tissues of growing
99 maize roots (Kozlova *et al.*, 2019).

100

101 The aim of the present work was to measure changes in the indentation modulus of each cell wall
102 layer during the maturation of poplar tension wood fibres using AFM. As it was not possible to
103 monitor the maturation of a single cell over time, as a proxy, we chose to perform measurements on
104 several cells in the same row, from cambium to mature wood, that were therefore at different stages
105 of development. Using the kinetics of cell wall thickening as a basis for comparison, the stiffening of
106 the different layers of the cell wall was compared to other known phenomena such as changes in
107 mesoporosity and in crystalline cellulose strain. In addition, thanks to the nanometric spatial
108 resolution of AFM measurements, we investigated G-layer stiffening during thickening, i.e., the
109 kinetics of stiffening within the G-layer, and fluctuations in the mechanical states of a new freshly
110 deposited sub-layer. Finally, the kinetics and stiffness gradient of the poplar G-layers were compared
111 with data available in the literature on bast (primary phloem) and xylem flax fibres, whose cells walls
112 contain both a thick immature G_n-layer and a mature G-layer (Goudenhoofft *et al.*, 2018; Petrova *et*
113 *al.*, 2021).

114 **Materials and methods**

115 *Sample preparation*

116 The experiments were conducted on a wood sample cut out of a young poplar tree tilted to induce the
117 production of tension wood. This hybrid poplar plant (*Populus tremula* × *Populus alba*, INRA clone
118 717-1-B4), was grown in controlled greenhouse conditions for two months (INRAE, Orléans, France)
119 before being tilted to trigger the formation of tension wood on the upper side of its stem. Twenty-two
120 days after tilting, a 5-cm long stem section (estimated diameter 1 cm) was collected at the base of the
121 stem, a few cm above the ground. Small wood sub-samples a few mm in size were cut out of the
122 tension wood side and fixed for 4 h in 2.5% formaldehyde and 0.1% glutaraldehyde in 0.1M
123 McIlvaine citrate-phosphate buffer, pH 6.8, followed by 3×10 min under moderate vacuum. After
124 thorough rinsing in McIlvain buffer, the sample was partially dehydrated in increasing series (25%,
125 50%, 70%) of ethanol and progressively impregnated with LR-White medium grade resin (London
126 Resin Company Ltd, UK) in a series of resin and ethanol mixes containing a progressively increasing
127 percentage of resin (20% 2h, 40% 4h, 60% 4h, 80% 24h, 100% 2+8 days). During the last pre-
128 embedding step, in pure resin, the sample was placed under moderate vacuum for 3×10 minutes.
129 Finally, the samples were embedded in gelatine capsules filled with pure resin and heated in an oven
130 at 56 °C for 24 h for polymerization. Semi-thin transverse sections (0.5 to 1 µm) were cut with a
131 Histo diamond knife (Diatome Ltd, Nidau, Switzerland) installed on a Ultracut S microtome (Leica
132 Microsystems, Vienna, Austria) to trim the block. To avoid the deformation commonly observed in
133 G-layers as a result of swelling, detachment and collapse after stress release (Clair *et al.*, 2005a;
134 2005b), at least the first 50 µm of the sample were trimmed and discarded. Finally, very thin sections
135 (about 50 nm thick in the last step) were made at a low cutting speed (≈1 mm/s) using an Ultra AFM
136 diamond knife (Diatome) to obtain a nearly perfect flat surface. AFM measurements were carried out
137 on the remaining block.

138

139 *Optical measurement of the cell wall layer thickness*

140 After AFM experiments, semi-thin transverse sections (0.9 µm) were cut with a Histo diamond knife
141 (Diatome) installed on an Ultracut R microtome (Leica Microsystems). These sections were stained
142 using Richardson's azur II and methylene blue (Richardson *et al.*, 1960) and mounted on slides using
143 Canada balsam. The slides were observed under a light microscope (DMLP, Leica Microsystems)
144 with immersion oil lenses (Fig. 1). Phase contrast microscopy is preferable to bright field microscopy
145 when observing the cell wall layer with high magnification (×600) as the specimen is thin, so the
146 colour contrast is reduced (Abedini *et al.*, 2015). Several images were acquired using a light
147 microscope with a digital camera (DFC320, Leica Microsystems) from the cambium to a distance of

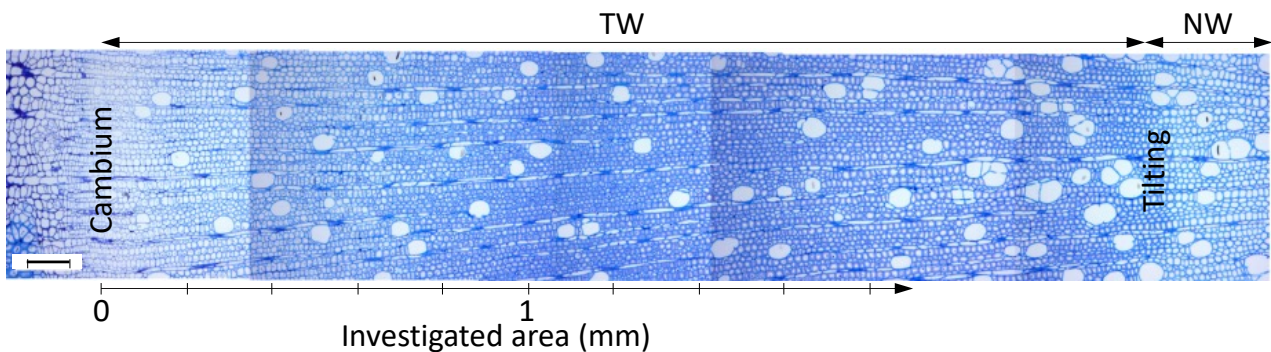
148 about 2 mm from it on the xylem side (i.e., with fully matured fibres), with a sufficient overlap to
149 allow the image to be repositioned to accurately measure the distance of each cell from the cambium.
150 The mean thickness of the S₂ and G layers was measured all along two radial rows using Matlab
151 software (MathWorks Inc., Natick, Massachusetts, USA) according to the method of Yoshinaga *et al.*
152 *et al.* (2012). External contours of the lumen, S₂ and G layers were plotted by hand from images and
153 their average thickness was calculated as (Abedini *et al.*, 2015):

$$154 \quad Th_G = \frac{2A_G}{P_G + P_{lumen}}, \quad (2)$$

$$155 \quad Th_{S_2} = \frac{2A_{S_2}}{P_{S_2} + P_G}, \quad (3)$$

156 where A_G and P_G are the area and the external perimeter of G-layer, respectively, A_{S_2} and P_{S_2} are the
157 area and the external perimeter of the S₂ layer, respectively, and P_{lumen} is the lumen perimeter. The
158 data presented in this article show the thickness of each layer normalized by the mean cell diameter,
159 D , which was evaluated as $D = \frac{P_{S_2}}{\pi}$. The advantage of working with relative thickness is that it allows
160 the effect of the fibre ends on the cell wall thickness to be corrected (Okumura *et al.*, 1977; Abedini
161 *et al.*, 2015).

162



163

164 *Fig. 1. Optical image of the transverse section of the wood sample (Richardson's staining) with the*
165 *tension wood (TW) area between the cambium and the normal wood (NW) produced before the tree*
166 *was tilted. The reference distance from the cambium was measured approximately in the middle of*
167 *the cambial zone. Scale bar = 0.1 mm.*

168

169 *AFM PF-QNM measurements*

170 Mechanical characterisation was performed with a Multimode 8 AFM (Bruker Corporation, USA) in
171 PF-QNM imaging mode with a RTESPA-525-30 (Bruker) probe. The spring constant of the probe
172 was calibrated by Bruker using a laser Doppler vibrometer with a value of 158 N/m. The initial tip

173 radius, 33 nm (controlled by Bruker), was checked after adjusting the cantilever deflection sensitivity
174 on sapphire and corrected to 40 nm to obtain the right range of indentation modulus on the centre of
175 DuPont™ K48 Kevlar® fibres (~20 GPa) embedded in Struers Epofix epoxy resin (~4 GPa), as
176 described in Arnould *et al.* (2017). The value of the tip radius was checked indirectly and, if
177 necessary, corrected using the above-mentioned calibration sample by ensuring that the indentation
178 modulus and the adhesion force in the embedding resin of the wood sample remained constant around
179 the wood sample and within the lumen in the cambial area. After all the measurements, the final tip
180 radius was 120 nm. The applied maximum load was set at 200 nN for all the measurements, the
181 vertical motion for force-distance curves was set at a frequency of 2 kHz, and the fast scan rate was
182 such that the scan speed was always equal to 8 $\mu\text{m/s}$ regardless of the size of the image (512×512
183 pixels), with a scan axis angle of 90° .

184
185 The force-distance curves obtained were automatically adjusted by a Derjaguin-Muller-Toporov
186 (DMT) contact model (Derjaguin *et al.*, 1975) to obtain the indentation modulus using Nanoscope
187 Analysis software (Bruker), with an assumed spherical tip, a flat sample surface, and taking the
188 measured adhesion force into account. This model is one of the simplest and is suitable for vitreous
189 polymer resin and all wood cell wall layers, considering the relatively low values of their Tabor
190 parameter (Johnson and Greenwood, 1997; Xu *et al.*, 2007). The discernible layers, i.e., layers that
191 are thick enough to avoid the measurement being influenced by edge or topography effects, are the
192 cell corner middle lamella (CCML), S_1 with the primary wall (i.e., S_1 -P, as in most cases, these two
193 layers are almost impossible to distinguish), S_2 and G layers. For each of these layers, the indentation
194 modulus distribution was obtained using Gwyddion freeware (<http://gwyddion.net/>). This distribution
195 can be adjusted with a Gaussian function that gives the value at the maximum of the distribution (i.e.,
196 mode or most frequent value in the dataset) and the standard deviation of the indentation modulus.
197 Measurements were made on three different radial rows of developing cells in the wood sample, one
198 after the other, always starting from the cambium and continuing up to a distance of about 1.7 mm
199 away, with two overlapping sets of measurements for the first row to check the stability and
200 repeatability of the measurements. Twenty-four different positions (and thus cells) were measured in
201 the two first radial rows and 12 positions in the last row. As soon as it was visible, the thickness of
202 the S_2 and G layers was measured using the same protocol as for the optical images. To complete our
203 study and to have a reference, we measured the indentation modulus and the thickness of the cell wall
204 layers in three normal wood cells (one per radial row) that had differentiated before the tree was tilted
205 and were therefore devoid of a G-layer. All the data were assembled using Matlab software (The
206 MathWorks Inc., Natick, Massachusetts, USA).

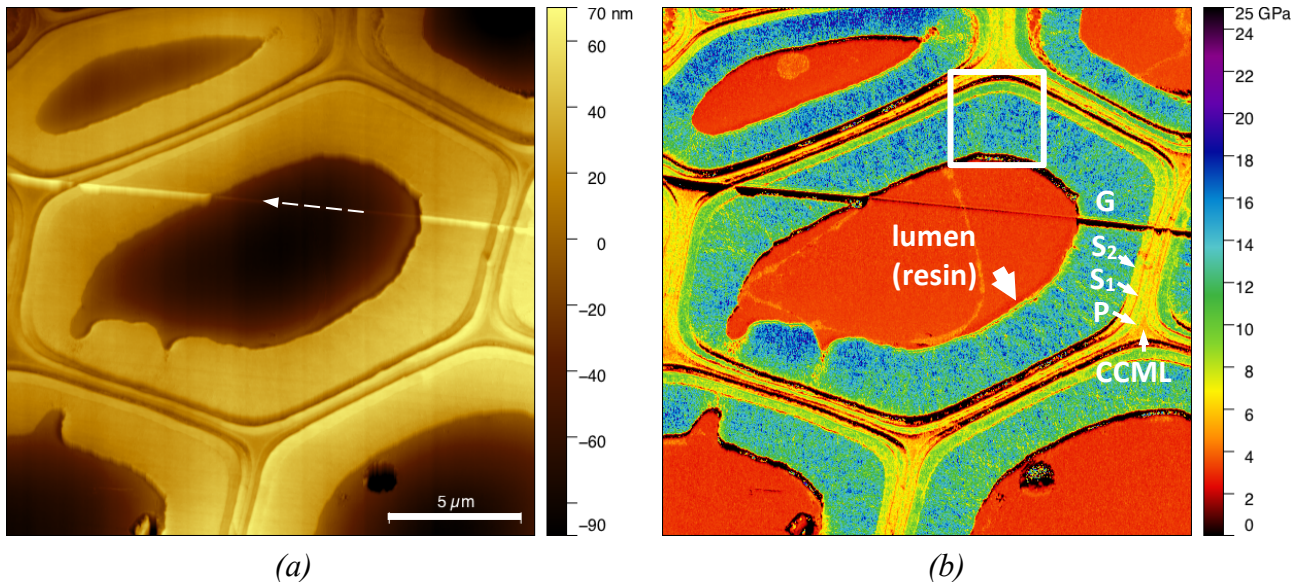
207

208 Finally, the AFM values were checked by nanoindentation measurements on a few cells located
209 700 μm from the cambium using iNano KLA nanoindenter (Scientec, Les Ulis, France) in mapping
210 mode (NanoBlitz) on a $200 \times 200 \mu\text{m}$ (20×20 pixels) area, with a maximum force of 0.1 mN and a
211 loading frequency of 1 Hz.

212

213 Results

214 Mapping the indentation modulus of developing fibres



215

216 *Fig. 2. PF-QNM mapping of (a) topography and (b) indentation modulus of the cross section of a*
217 *tension wood fibre 740 μm from the cambium (first radial row). The different layers are identified: P*
218 *stands for primary wall and CCML for cell corner middle lamella. The lumen of the cell was filled*
219 *with LR-White resin. The white dashed arrow in (a) shows the microtome cutting direction (following*
220 *a scratch line due to imperfections of the diamond knife), the thick white arrow in (b) points to a thin*
221 *and softer sub-layer that corresponds to the white upper box in (b) and is discussed in more detail in*
222 *Fig. 4.*

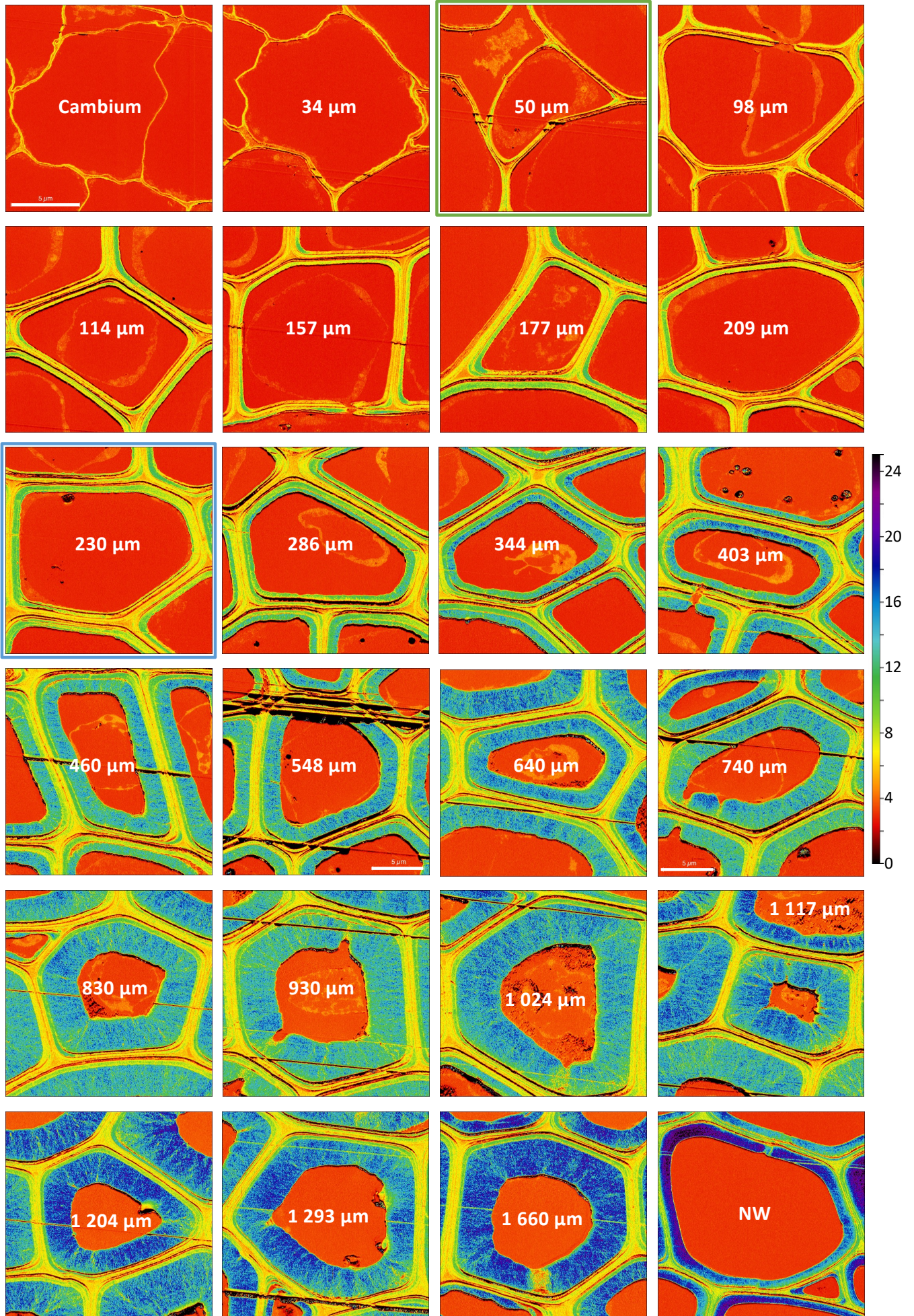
223

224 The AFM measurements provided a map of the sample topography and a map of the indentation
225 modulus. Examples of typical maps obtained for a cell are given in Fig. 2, at a distance of 740 μm
226 from the cambium (first radial row). The different layers of the cell wall (cell corner middle lamella
227 CCML, primary cell wall P, secondary cell wall S₁, S₂ and G-layers) are clearly identifiable on the
228 indentation modulus map due their different elastic mechanical properties. Note that part of the cell
229 contents in the lumen are identifiable (Fig. 2b), while they are not visible in the topography (Fig. 2a).
230 The different cell wall layers are also quite easy to distinguish on the topography map because of the

231 slight change in height between each layer. The height is almost uniform within the G-layer, middle
232 lamella and embedding resin in the lumen, whereas it varies around the circumference in the S₁-P and
233 S₂ layers. These variations are the opposite in the S₁-P and S₂ (S₁-P is high when S₂ is low) and these
234 extreme values were obtained perpendicular to the cutting direction (white dashed arrow in Fig. 2a).
235 These observations are typical of a cutting effect as previously described in Arnould and Arinero
236 (2015). Moreover, we observed limited orthoradial variations in the indentation modulus of the S₂-
237 layer around the cells. This proves that the wood fibres are rather well oriented perpendicular to the
238 cutting direction and that there will be little (or even no) bias in the interpretation of the measurements
239 due to sample misalignment (Arnould and Arinero, 2015).

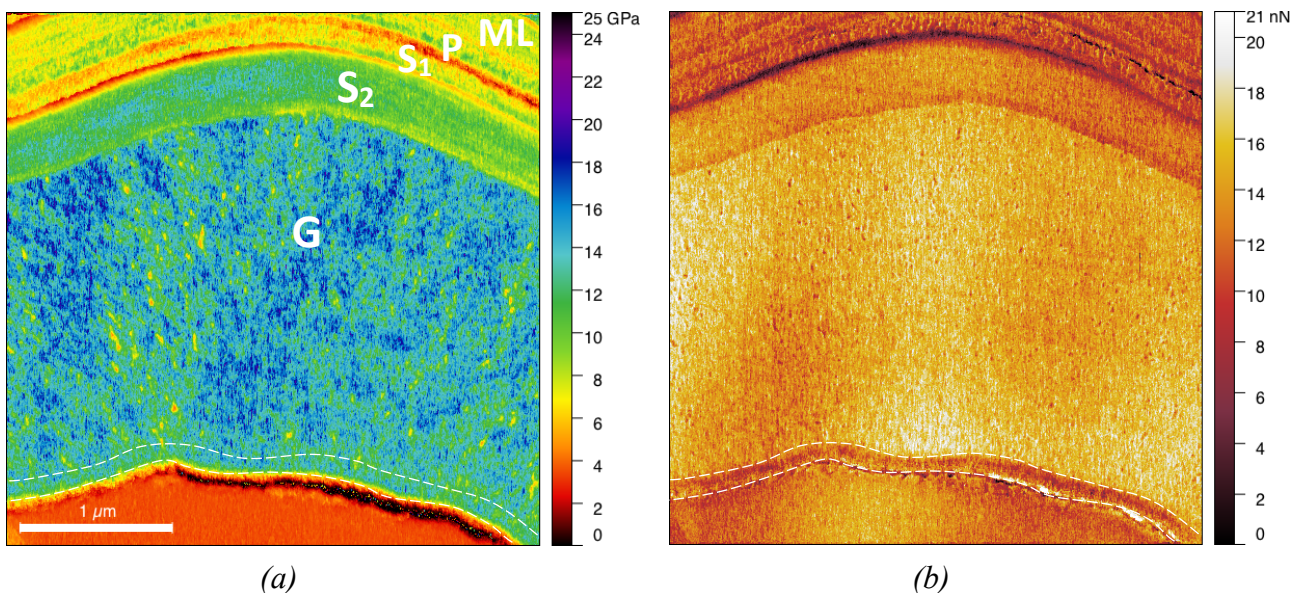
240
241 Fig. 3 shows the mechanical maps of all the cells measured in the first radial row. Progressive
242 thickening of the cell wall results in the appearance of the different layers of the secondary wall: the
243 first distinguishable S₂ appears around 50 µm from the cambium (map with the green border in Fig.
244 3) and first distinguishable G-layer around 230 µm from the cambium (map with the blue border in
245 Fig. 3). A continuous increase in the indentation modulus of the embedding resin is visible in the
246 lumen from 2.7±0.1 GPa in the cambium to 3.4±0.2 GPa at 1.7 mm. This increase was not observed
247 in the embedding resin outside the wood sample where the indentation modulus remained equal to
248 around 2.7±0.1 GPa in all the measurements. Moreover, immediate measurement of the indentation
249 modulus of the embedding resin in the lumen of cells in the cambium taken just after the last measured
250 cell in a given row, showed a return the initial value of 2.7±0.1 GPa.

251
252 The indentation modulus obtained for the S₂-layer of normal wood cells 2 mm from the cambium,
253 was around 16.9±5.5 GPa and its relative thickness was around 0.055 (see NW in Fig.3). A more
254 pronounced variation of the indentation modulus was observed in the S₂-layer of this cell, which is
255 probably due to a slight misorientation of the fibre with respect surface as already described in
256 Arnould and Arinero (2015). The indentation moduli of the other layers were 7.5±1.2 for the CCML
257 and 8.2±3.1 GPa for the S₁-layer, while the indentation modulus in the embedding resin in the lumen
258 was 2.99±0.21, a value close to that recorded in the cambium or outside the wood sample. The
259 indentation modulus was confirmed by nanoindentation in the embedding resin in the lumen and in
260 the G-layer of a few cells 700 µm from the cambium with a value of 3.5±0.15 GPa and 13.5±1.3 GPa,
261 respectively (see Fig. S3 and Table 1 for comparison).



263 Fig. 3. Indentation modulus maps of the different cells measured in the first radial row. The white
 264 number in the lumen refers to the distance of the cell from the cambium, the cells are arranged in
 265 rows from left to right and from top to bottom, with the cambium always on the left. The last map on
 266 the bottom right shows a normal wood (NW) cell, here before tilting (Fig. 1). The map at 50 μm
 267 (green border) is the first map with a distinguishable S_2 -layer. The map at 230 μm (blue border) is
 268 the first map with a distinguishable G-layer. Except for the maps at 548 and 740 μm , the size of the
 269 maps is same in all the images. Scale bar = 5 μm .

270
 271 Overall stiffening of the G-layer with increased distance from the cambium was clearly visible. A
 272 radial pattern (radial lines in the cell wall) was also visible in the G-layer, as previously reported by
 273 Sell and Zimmermann (1998). Some ring lamellae were also visible within the cell wall layers (e.g.,
 274 at 548, 740, 830, 930, 1024 and 1660 μm from the cambium in Fig. 3 and in the enlargement of
 275 Fig. 2b in Fig. S1). This last structural pattern is consistent with the radial layer-by-layer thickening
 276 of the wall and has been already reported, for example, in the S_2 -layer of wood fibres (Fahlén and
 277 Salmén, 2002; Casdorff *et al.*, 2018), in the G-layer of most *Salicaceae* species excepted in the poplar
 278 genera (Ghislain *et al.*, 2016), in mature (Hock, 1942) and in developing G-layers of flax bast fibres
 279 (Arnould *et al.*, 2017; Goudenhooff *et al.*, 2018) and in mature hemp fibres with a G-layer (Coste *et*
 280 *al.*, 2020).

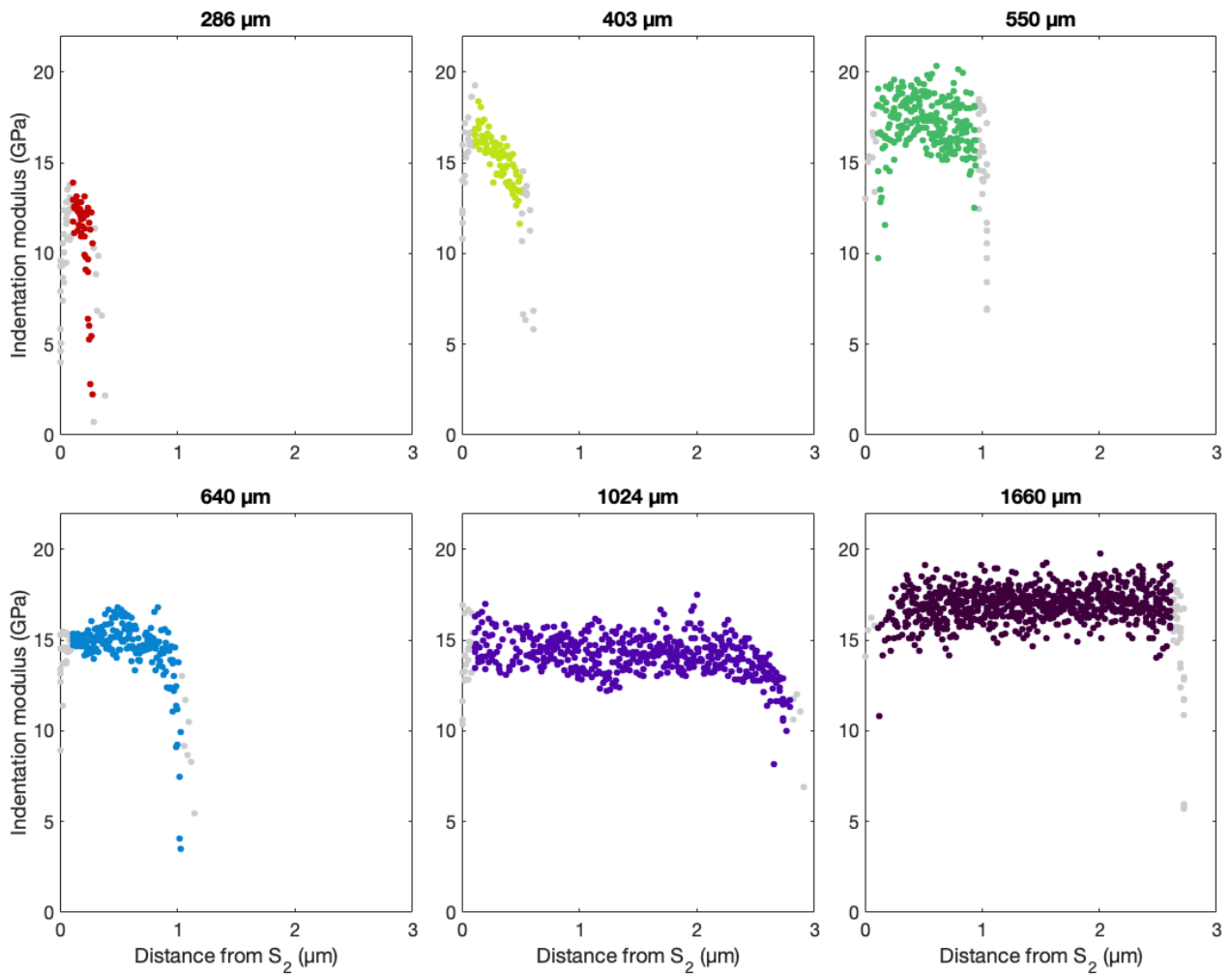


281
 282 Fig. 4. a) Close-up of the indentation map of a cell taken at a distance of 740 μm from the cambium
 283 corresponding to the white box in Fig. 2b with the associated adhesion map (b) highlighted sub-G-
 284 layer with lower adhesion force close to the lumen.

285

286 At a distance from the cambium equal to or greater than 440 μm , a thin and soft sub-layer was visible
287 on the lumen side at the border of the G-layer but only on the right side of the map (as shown in
288 Fig. 2b). The fact that this sub-layer is only visible on the right side of all cells can be attributed to a
289 cutting effect when the sample surface was prepared with the diamond knife, as the cutting direction
290 is almost horizontal and proceeds from the right to the left (see Fig. 2a). As cutting effects are linked
291 to the mechanical behaviour of the cell wall, this sub-layer reveals a different behaviour than the rest
292 of the G-layer. The average indentation modulus of this sub-layer was around 8.2 ± 2.6 GPa, close to
293 the value of the early G-layer, at a distance of 230-286 μm from the cambium, and its thickness was
294 around 100 nm in all cases. Fig. 4a gives a closer view of the G-layer at the top of the cell at 740 μm
295 from the cambium (white box in Fig. 2b) and Fig. 4b is the adhesion map. Although the sub-layer is
296 not visible on the indentation map in Fig. 4a, a sub-layer with a thickness of around 100 nm and a
297 lower adhesion force than the rest of the G-layer is also visible on the border of the lumen in Fig. 4b.
298 We can assume that it is the same sub-layer as that observed on the right side of the indentation
299 modulus maps. Moreover, its low adhesion force is close to that of the early G-layer (see Fig. S2).

300
301 To further investigate the kinetics of G-layer stiffening, from six fibres situated at different distances
302 from the cambium, we extracted six to ten radial profiles of the indentation modulus around the cell
303 axis in the G-layer (Fig. 5). Each point in a radial profile is the average of the modulus over a width
304 of 10 pixels. To reduce possible bias in the interpretation of the data caused by an edge effect due to
305 cutting with the diamond knife or an effect of the area mechanically sensed by the tip (Sudharshan
306 Phani and Oliver, 2019), we removed the first and last 100 nm from each profile (data points in grey
307 in Fig. 5). In contrast to the indentation modulus map in Figs. 2b and 3, where no mechanical gradient
308 is visible in the developing G-layers, here a gradient was always visible on the last 500 nm or so on
309 the lumen side and became less pronounced with an increase in the distance from the cambium. The
310 gradient completely disappeared in the mature fibre (see Fig. 5 at 1 660 μm). It was not possible to
311 determine whether such a gradient existed in the S₂-layer because, even if it were present, it would
312 be hidden by the effect of the apparent microfibril angle due to the slight misalignment of the sample
313 (Arnould and Arinero, 2015).



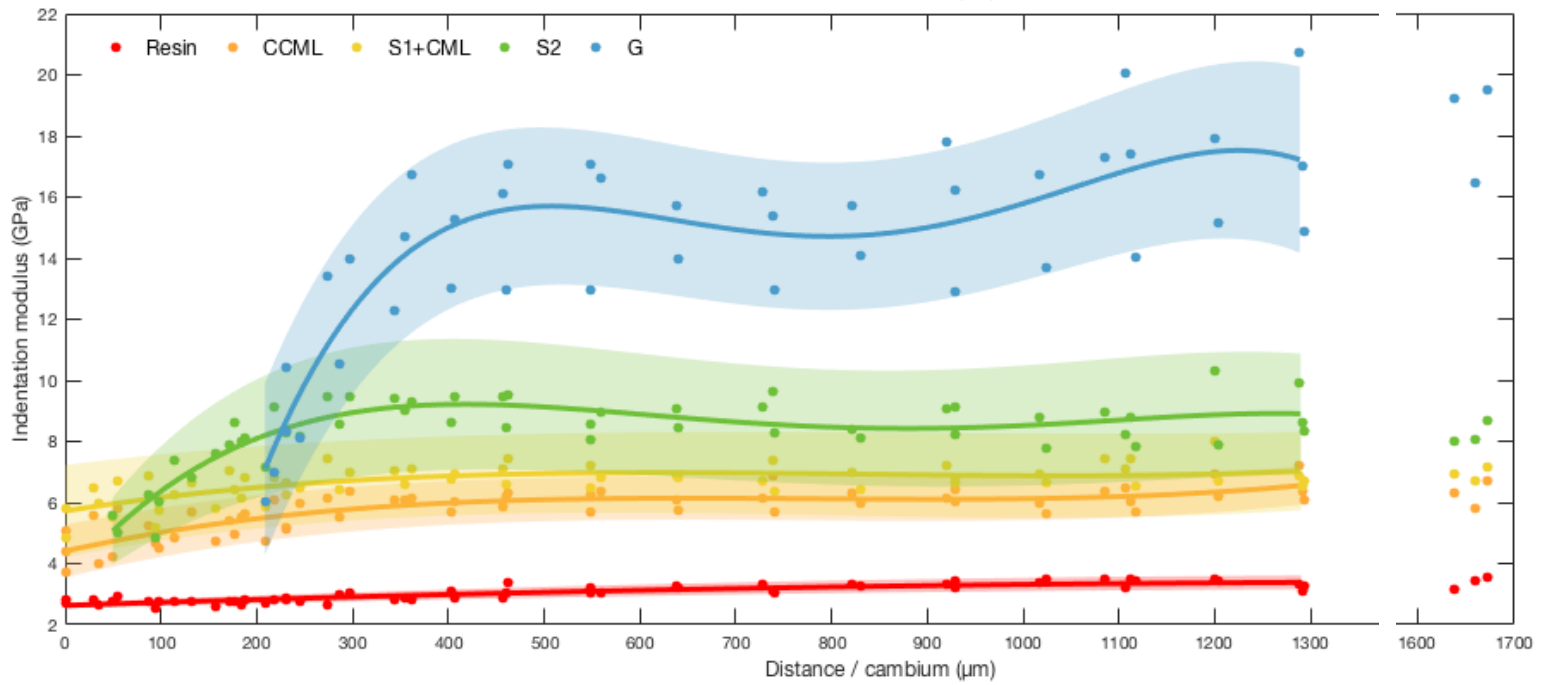
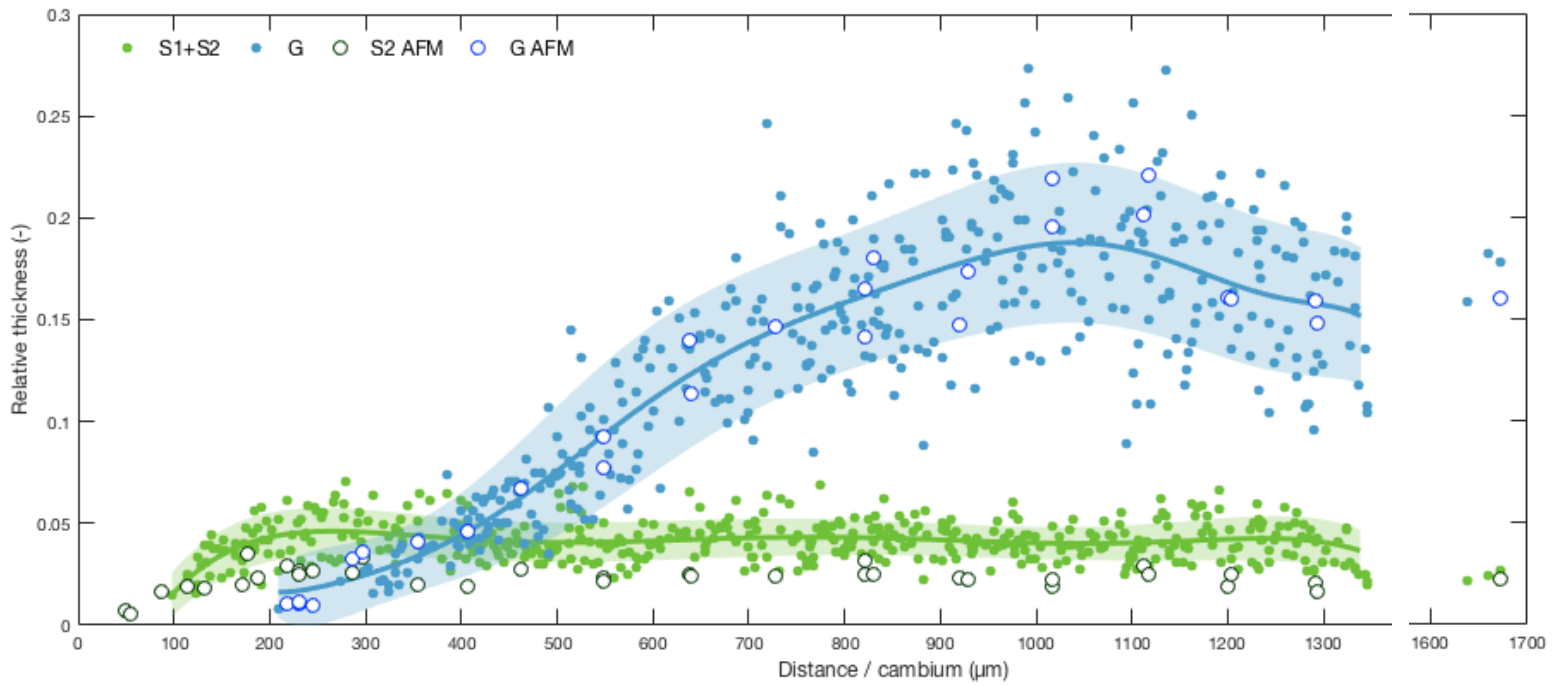
314

315 *Fig. 5. Observation of the occurrence of a radial mechanical gradient during the maturation of the*
 316 *G-layer obtained by extracting radial profiles all around the cell axis in this layer and plotting them*
 317 *as a function of the distance from the S₂ layer for six different distances from the cambium (value*
 318 *given at the top of each graph). The first and last 100 nm were removed from each profile (data points*
 319 *in grey) to avoid any bias due to measurement edge effects.*

320

321 ***Dynamics of global cell-wall layer thickening and stiffening***

322 All the observations made above were also made in the 2nd and 3rd radial rows. Changes in the mode
 323 of the indentation modulus distribution in each layer (e.g., see Fig. S3) are shown in Fig. 6, as a
 324 function of the distance from the cambium, together with the relative thickness of each layer. In fig. 6,
 325 one point corresponds to one cell, whatever the radial rows, the continuous line corresponds to the
 326 mean trend adjusted on these points by a polynomial fit and the coloured ribbon to this fit shifted
 327 vertically by plus or minus the mean standard deviation on each layer of the cell wall.

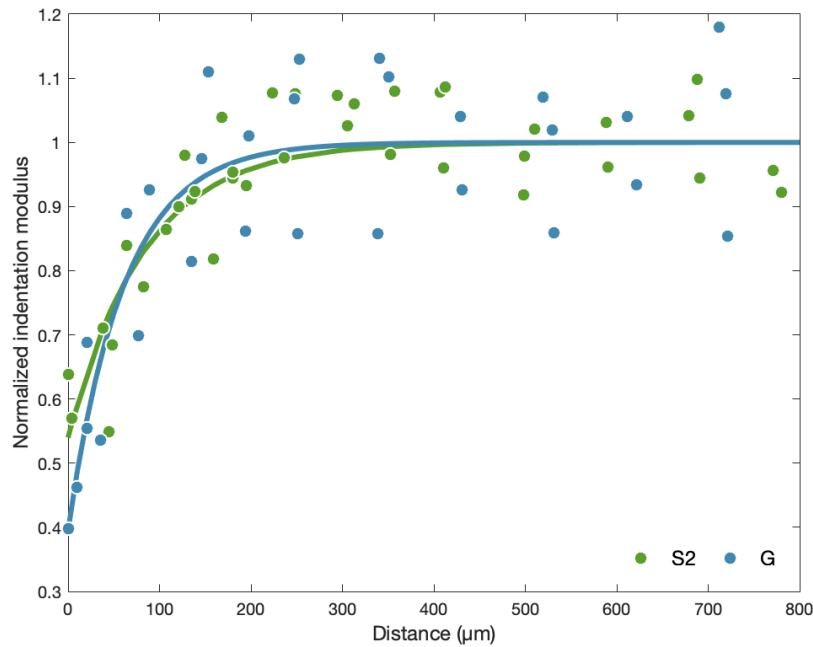


329 *Fig. 6. Variations in the relative thickness of the cell wall layers measured by optical microscopy*
330 *(coloured dots) and AFM (empty circles) (top) and mode of the indentation modulus distribution*
331 *(bottom), as a function of the distance from the cambium. The solid lines and the shaded areas show*
332 *the mean tendency and standard deviation adjusted on these points.*

333 In the case of the optical measurements of the thickness of the layers, it was not possible to separate
334 the S₁ and S₂ layers, unlike for the AFM measurements. The measurements of relative thickness made
335 by optical microscopy and AFM are consistent, but AFM enables detection of the appearance of the
336 cell wall layer and its thickening earlier than optical microscopy. The thickness of the S₂ alone
337 obtained by AFM is thus logically smaller than S₁+S₂ obtained by light microscopy. The relative
338 thickness of the S₂-layer increases until around 200 μm from the cambium then decreases a little
339 before reaching a stable value at a distance of around 500 μm from the cambium. The G-layers were
340 first detected close to 200 μm from the cambium. The relative thickness of the G-layer increased
341 linearly and stabilised near 1 000 μm. Thus, the relative thickness of S₂ was slightly higher before the
342 appearance of the G-layer.

343
344 A progressive increase in the indentation modulus of both the CCML (from 4.6±0.7 to 6.1±0.7 GPa)
345 and the S₁ layers (from 5.6±1.5 to 6.8±1.3 GPa) was observed until the end of the S₂ stiffening, at
346 around 350 μm from the cambium. The very first S₂-layers had indentation moduli of 5.1±1.4 GPa
347 and their stiffening and their thickening were initially synchronous. Later, when the S₂-layers reached
348 their final thickness, their indentation modulus continued to increase and finally reached a value of
349 8.7±2.0 GPa. All these layers continued to stiffen when the G layer began to thicken. In contrast, the
350 global stiffness of the G-layer was almost stable (at around 500 μm from the cambium) long before
351 it reached its final maximum thickness (at around 1 000 μm from the cambium).

352
353 As already mentioned, as these curves correspond to the mode of the indentation modulus distribution
354 (i.e., value at the maximum of the distribution or most frequent value, see Fig. S3), they do not reflect
355 the gradient observed at about 500 nm from the edge of the G-layer on the lumen side due to the
356 progressive maturation of a potentially freshly deposited sub-G-layer (Fig. 5). Furthermore, as shown
357 in Fig. 5, the thickness of the G-layer at 550 μm from the cambium is such that most of the G-layer
358 has completely stiffened, leading to the stabilised value of the indentation modulus reported in Fig. 6
359 for this distance from the cambium.



360

361 *Fig. 7. Normalized indentation modulus of the S₂ and G-layers from Fig. 6 as a function of the*
 362 *distance from the cell where the layer concerned first appeared. The solid line corresponds to the*
 363 *mean value.*

364

365 To compare the dynamics of the stiffening of the S₂ and G-layers, Fig. 7 shows the normalized
 366 indentation modulus (i.e., the modulus from Fig. 6 divided by its mean maximum value) as a function
 367 of the distance from the cell where the layer concerned first appeared (i.e., 50 μm from the cambium
 368 for S₂ and 230 μm for G-layers, Fig. 3). This figure shows that the dynamics of the two layers are
 369 quite similar, i.e., it took a distance of around 250 μm to reach their mature modulus. However, it
 370 appears to be faster for the G-layer as the change in modulus from the first deposited layer to the final
 371 mature one is larger.

372

373 Discussion

374 Our main results revealed: i) initial synchronous stiffening of the CML, S₁ and S₂-layers with the
 375 thickening of the S₂-layer, which continues a little after the S₂-layer has reached its final thickness
 376 while the G layer starts to develop; ii) initial global stiffening of the G-layer synchronous with its
 377 thickening but stable global stiffness reached long before its final maximum thickness; iii) a stiffness
 378 gradient over about 500 nm on the lumen side in the developing G-layer with a softer sub-layer at the
 379 lumen edge about 100 nm in thickness.

380

381 *Potential effects of sample preparation on the measurements*

382 The different steps of sample preparation protocol made it impossible to keep the sample in its native
383 *in planta* green state: we thus cannot rule out the possibility that modifications of the different layers
384 of the cell wall during the ethanol exchange and resin embedding had some impacts on its mechanical
385 properties but, for the reasons detailed below, we believe that we achieved a good compromise.
386 Indeed, this preparation was necessary to ensure reliable mechanical measurements at small scale by
387 AFM. Since all the measurements had to be comparable, this treatment minimised artifacts caused by
388 roughness of the sample surface (Peaucelle, 2014). Indeed, mechanical measurements based on
389 indentation require samples with a surface that is as flat as possible, compared to the radius of the
390 AFM tip, to enable the use of reliable and simple contact mechanics models. These models are needed
391 to extract the indentation modulus from the contact stiffness (Arnould and Arinero, 2015) or from the
392 force-distance curves (Hermanowicz *et al.*, 2014). In addition, the AFM tip is very brittle and surface
393 roughness has to be as low as possible to reduce the risk of tip wear or breakage: this is especially
394 important in the present study where we had to perform many measurements using the same probe to
395 limit measurement bias or drift. AFM measurements at such a small scale are only sensitive to the
396 very near sample surface. Damage during preparation of the sample surface should therefore be
397 reduced to the strict minimum. In addition, as we expected to find evidence for the existence of a
398 mechanical gradient during the thickening of the cell wall layers, we had to begin taking
399 measurements as close as possible to the cambium, where the cell wall is very thin and soft. This is
400 only possible when the sample has been previously embedded to avoid, or at least reduce, deformation
401 and damage during cutting and measurements. In addition, cell wall thickening progresses from the
402 lumen side of the cell wall and, without embedding, measurements made close to the lumen would
403 be highly modified due to border effects (Jakes *et al.*, 2008; Jakes *et al.*, 2009) unless the lumen is
404 filled with a sufficiently stiff substance such as resin. Finally, these embedding steps reduce cell wall
405 layer deformation during the cutting process and avoid swelling, detachment and collapse of the G-
406 layer commonly observed after stress release (Clair *et al.*, 2005a; 2005b).

407
408 Other studies have shown that LR-White embedding resin has little impact on the mechanical
409 properties of the cell wall due to very limited penetration into the cell wall of normal wood (Coste *et*
410 *al.*, 2021) and *a priori* in the G-layers of tension wood (Arnould and Arinero, 2015) and of other
411 similar fibre cell walls such as in flax (Arnould *et al.*, 2017) and hemp (Coste *et al.*, 2020). What is
412 more, the use of ethanol is expected to cause only slight deformation of the wall. For example, Chang
413 *et al.* (2012) showed that ethanol dehydration produced longitudinal macroscopic shrinkage of only
414 0.2% and volumetric swelling of only 0.5%. It is possible to avoid ethanol dehydration by drying the

415 sample at moderate temperature just before embedding (Konnerth *et al.*, 2008). However, in the
416 present biomechanical context with the G-layer, such a drying step would lead to very significant
417 changes in the cell wall ultrastructure (such as mesoporosity collapse, Clair *et al.*, 2008).

418
419 The main impact of sample preparation on the mechanical properties of the cell wall is in fact its
420 potential effects on the moisture content of the different layers. Indeed, sample preparation probably
421 modified moisture content from a green state to close to an air-dry state. The effect of moisture
422 content on the mechanical properties of the different cell wall layers has already been measured by
423 nanoindentation in the cell corner middle lamella and the S₂ layer of different woody species using
424 samples that were embedded (Wagner *et al.*, 2015) or not (Bertinetti *et al.*, 2015; Meng *et al.*, 2015).
425 These studies revealed a similar trend with a reduction of the indentation modulus from one third to
426 one half for the S₂ layer and at least one half for the cell corner middle lamella, between an air-dry
427 and saturated state. A more recent study (Coste *et al.*, 2020), using AFM PF-QNM in similar
428 conditions to those used in our study, focused on the effect of the moisture content on the mechanical
429 properties of hemp sclerenchyma fibres (containing a thick G-layer with similar characteristics to
430 those of the tension wood G-layer) and xylem fibres. In their study, AFM measurements of all the
431 cell wall layers revealed no major differences between layers, with a reduction of the indentation
432 modulus of about one half when the relative humidity varied from 13% to 83%. If we extrapolate
433 these variations to our study, the indentation modulus values reported here are overestimated
434 compared to the values *in planta* but the relative differences observed between layers, or within a
435 layer (gradient), are most probably comparable to what happens in the tree.

436 437 *Indentation modulus and its variations in the different layers of the cell wall*

438 We observed an increase in the indentation modulus of the embedding resin in the lumen, with
439 increased distance from the cambium, but it goes back to values measured in the cambial zone in the
440 normal wood (before tilting) cells lumen. The origin of this increase during fibre maturation is not
441 yet understood but is unlikely to be due to wear of the AFM tip as demonstrated by the repeatability
442 of the measurements in the cambial cells performed after measurements of each row, which were also
443 identical to those obtained at the end of all measurements in the lumen of the normal wood cells or
444 in the resin outside the sample. Stiffening thus appears to be associated with the change in the contents
445 of the lumen with the maturation of the fibres (as shown in Fig. 3). In cambial cells, the plasma
446 membrane and cytoplasm are bound to the inner part of the cell wall. Cambial cells are highly
447 vacuolated, and the large vacuole pushes the cell organelles outwards. There is therefore little material
448 inside the lumen (vacuole contents), which may explain why the indentation modulus measured in

449 the resin in the centre of cambial cells is close to that measured in normal wood cells that have lost
 450 all their cell contents. Finally, Table 1 shows that our LR-White indentation modulus values were the
 451 lowest, but were confirmed by nanoindentation. This is probably due to differences in the calibration
 452 procedure between laboratories or to the variability of the resin itself, as different grades (soft,
 453 medium, and hard) of this resin are available.

454
 455 The values of the indentation modulus in the different layers and the embedding resin are consistent
 456 with the (rather scattered) AFM data or nanoindentation measurements of wood cell walls available
 457 in the literature (Eder *et al.*, 2013), although in the low range compared literature data on the G-layer
 458 of poplar or tension wood (see Table 1). These low values can probably be partly explained by the
 459 fact that the tree used in our study was young (less than 3-month old), and the juvenile wood it
 460 produced had a high microfibril angle (MFA) in the S₂-layer and low cellulose content (Luo *et al.*,
 461 2021), and the fact that the cell used as an example in Fig. 2 was not fully mature. The values of the
 462 indentation modulus in the G-layer of a mature cell increased to around 18.3±3.1 GPa on average
 463 (see Fig. 6), a value similar to the literature data listed in Table 1.

464
 465 *Table 1. Comparison of the value of the indentation modulus (in GPa) in the different layers of mature*
 466 *wood fibres in our study and in the literature.*

Reference	LR-White				
	resin (lumen)	ML (CC)	S ₁	S ₂	G
This study, developing tension wood (740 µm, Figs. 2 and S2)	3.10±0.29	5.4±1.0	6.5±1.4	8.3±2.2	13.0±3.1
This study, mature tension wood (1660 µm, Fig. 3)	3.35±0.27	5.9±1.0	6.7±1.2	8.2±2.6	16.5±3.3
This study, mature normal wood (NW, Fig. 3)	2.99±0.21	7.5±1.2	8.2±3.1	16.9±5.5	n.a.
Normand <i>et al.</i> (2021) (poplar)	3.9±1.8	9.9±1.2	11.3±0.3	16.4±0.4	16.8±0.5
Clair <i>et al.</i> (2003) (oak, no embedding)	n.a.	5-7	8-9	9-10	10-12
Arnould and Arinero (2015) (chestnut)	3.5±1.5	6±0.5	n.a.	13±0.5	15±1.5
Liang <i>et al.</i> (2020) (poplar, no embedding)	n.a.	n.a.	6.89- 10.48	10.57- 14.61	11.13- 18.5
Coste <i>et al.</i> (2021) (poplar)	4.5±0.9	10.7±2	16.0±3.8	18.2±3.5	n.a.

467

468 The low value obtained for the mature S₂-layer in the tension wood area compared to the value in
469 normal wood can be explained by a marked difference in MFA between the S₂-layers of normal wood
470 (with a low MFA and therefore a high indentation modulus) and the S₂-layers of tension wood (with
471 a high MFA and therefore a small indentation modulus, Eder *et al.*, 2013; Jäger *et al.*, 2011). To
472 explain this difference (equal to a factor of about 2) between the indentation moduli, we can roughly
473 estimate from published data that the MFA is around 5-10° in normal wood whereas it is 30-40° in
474 the S₂ of tension wood (Arnould and Arinero, 2015; Jäger *et al.*, 2011). This is also in agreement with
475 the value of MFA reported for the S₂-layer in tension wood for poplar by Goswami *et al.* (2008).
476 Likewise, the order of magnitude of the values of indentation modulus obtained for the different
477 layers of normal wood is in agreement with other literature data (Table 1).

478

479 *Dynamics of global thickening and stiffening of the cell-wall layers*

480 The CCML, S₁ and S₂-layers continued to stiffen while G-layer was developing (Fig. 6). This is in
481 agreement with the fact that the lignification of S₁, S₂-layers and CCML occurs during the formation
482 of the G-layer (Yoshinaga *et al.*, 2012). This lignification after the G-layer starts to thicken may be
483 explained by the presence of additional matrix material that has been transported through the existing
484 wall. Alternatively, some precursors may already be present and are used in biochemical reactions
485 that continue during the deposition of the G-layer. The effect of lignification on the mechanical
486 properties of the cell wall is not yet well understood, with different studies sometimes reporting
487 conflicting results, but recent studies tend to confirm the hypothesis that lignification mainly affects
488 the shear modulus and the strength of the matrix (Özparpucu *et al.*, 2017; 2019), with higher content
489 leading to a higher modulus and greater strength. As the indentation modulus is not only sensitive to
490 the longitudinal modulus but also to the transverse and shear moduli (Jäger *et al.*, 2011), which are
491 mainly influenced by the cell wall matrix, a change in the cell wall matrix properties due to
492 lignification causes a significative change in the indentation modulus, as already shown by
493 nanoindentation (Gindl *et al.*, 2002). Finally, Fig. 7 shows that the stiffening dynamics appear similar
494 although faster in the G-layer than in the S₂-layers suggesting that the physical and chemical changes
495 or reactions at work during cell wall maturation are faster in the G-layer (e.g., microfibrils aggregation
496 or gelatinous matrix swelling, Alméras and Clair, 2016) than in the S₂-layer (e.g., lignification).

497

498 The fact that the thickness of the S₂-layer decreases slightly when the G-layer is starting to develop
499 has already been observed. For example, Abedini *et al.* (2015) reported that this is a common trend
500 throughout the growing season in both normal and tension wood of poplar trees. Moreover, the
501 changes and mature value of the relative thickness of the G and S₂ layers in Abedini *et al.* (2015),

502 Chang *et al.* (2015) and Clair *et al.* (2011) are similar to our measurements. We therefore assume that
503 we can use the relative thickening of the different wall layer as a common spatial reference to link
504 different studies. If we combine our results with those of previous studies, the G-layer appears to
505 synchronously stabilise its thickness, whole indentation modulus (i.e., no more radial gradient), meso-
506 pore size (Chang *et al.*, 2015) and cellulose tensile strain (Clair *et al.*, 2011) at the end of the
507 maturation. These observations suggest that the different changes involved in the maturation process
508 of the G-layer start, evolve and end at approximately the same fibre development stage. These
509 physico-chemical observations now need to be coupled with biochemical analyses to better
510 understand the mechanisms involved in G-layer maturation, and possibly to establish relations
511 between matrix stiffening, bridging between microfibrils and wall compaction (Alméras and Clair,
512 2016; Gorshkova *et al.*, 2015; Mellerowicz and Gorshkova, 2012).

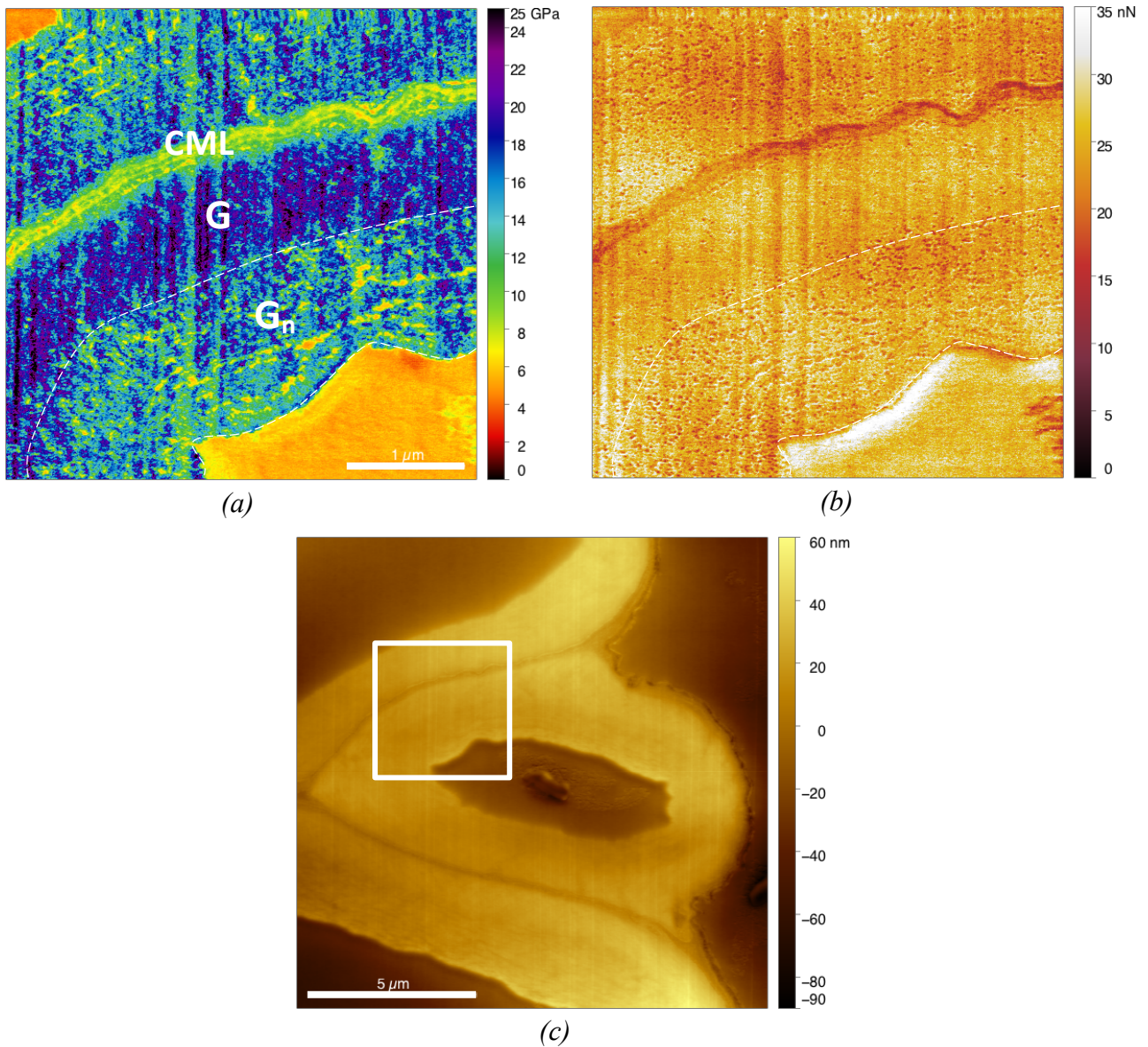
513
514 According to the radial profiles of the indentation modulus (Fig. 5), a smooth mechanical gradient
515 occurs in immature G-layer on less than 0.5 μm on the lumen side with a small sublayer of about
516 100 nm. This sublayer appears to be as dense as the mature part of the layer and could be either a
517 freshly deposited immature G-layer or part of the periplasmic area still bound to the layer. Indeed,
518 periplasmic area, located between the inner part of the G-layer and the plasma membrane, is the scene
519 of intense biochemical processes, see Fig. 2 in Pilate *et al.* (2004), Fig. 5 in Guedes *et al.* (2017) or
520 Fig. 7 in Decou *et al.* (2020). In contrast, flax bast fibres exhibit a strong mechanical gradient with a
521 thick immature, loose and soft G-layer, called G_n (Gorshkova and Morvan, 2006; Gorshkova *et al.*,
522 2010). Evidence for the presence of this thick G_n -layer has also been provided in flax xylem tension
523 wood fibres (Petrova *et al.*, 2021). Interestingly, the indentation modulus of flax G-layers is similar
524 to or even a little bit higher than that of mature poplar G-layers and the average indentation modulus
525 of flax G_n -layers is comparable to that measured in immature poplar G-layers in fibres close to the
526 cambium and to the inner sub-layers observed in more developed G-fibres.

527

528 *Comparison with flax G-layer*

529 The indentation modulus and adhesion force maps in the case of a typical developing flax fibre with
530 a sharp transition between G and G_n layers (Arnould *et al.*, 2017; Goudenhoft *et al.*, 2018) are shown
531 in Fig. 8. Several sublayers are observed as lamellae in the G_n , which exhibit indentation modulus
532 and adhesion force similar to those of the G-layer. These lamellae are separated by bands whose
533 indentation modulus is close to that of the resin, but with a lower adhesion force. This lamellar
534 arrangement is not observed in poplar, even though ring lamellae structure of this type is sometimes
535 discernible in the mature part of the G-layer (e.g., see cells at a distance of 548, 740, 830, 930, 1 024

536 and 1 660 μm μm from the cambium in Fig. 3 and Fig. S1). The most significant structure in the
537 poplar G-layer appears as radial bands (e.g., see tension wood cells at a distance of more than 740 μm
538 in Fig. 3). This pattern may reflect biological organisation, but we cannot exclude the possibility that
539 it is the consequence of (slight) shrinkage of the G-layer during dehydration with ethanol (Fang *et*
540 *al.*, 2007).
541

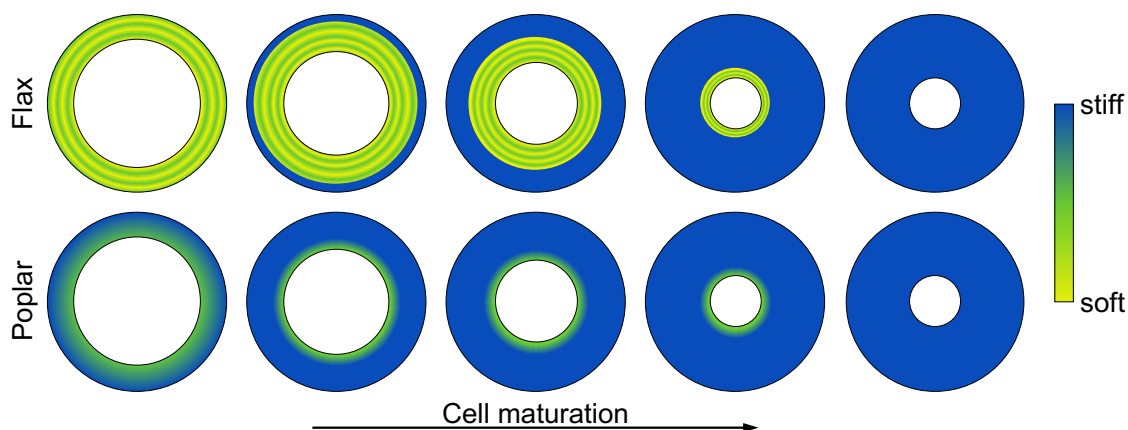


542
543 *Fig. 8. Comparison of the G and G_n-layers in developing flax bast fibre (60 days, half height of the*
544 *stem) adapted from Arnould et al. (2017): a) indentation modulus map and b) adhesion map*
545 *corresponding to the white box in the topography image (c).*

546
547 Note that it is impossible to compare the absolute value of adhesion forces obtained in the present
548 study (Fig. 4b) with the values obtained in Arnould *et al.* (2017) (in Fig. 8b) as this force depends to

549 a great extent on the on the shape of the tip and on the surface roughness of the material, which were
 550 not the same (see for example the difference in adhesion forces of the embedding resin in the lumen
 551 in the two studies, even though the same resin was used). In conclusion, although the G-layer of
 552 tension wood and the G-layer of flax are biochemically, ultrastructurally and mechanically similar
 553 (Coste *et al.*, 2020; Petrova *et al.*, 2021), here it is clear that they differ in their development and
 554 maturation, as summarised in Fig. 9, with a thick, loose, multilayer G_n layer in flax that stiffens and
 555 densifies abruptly, whereas in poplar, there appears to be a thin, dense immature layer that stiffens
 556 gradually. Thus, immunohistochemical and G-layer specific marker gene expression analyses (Decou
 557 *et al.*, 2020; Guedes *et al.*, 2017), like those already performed on flax bast and xylem fibres (Petrova
 558 *et al.*, 2021), should be performed on the same sample to clarify the origin of these differences and
 559 to better understand the mechanisms underlying the maturation and development of poplar tension
 560 wood growth stress. Finally, all these results should be used to distinguish between different models
 561 of growth stress development in the case of tension wood (Alméras and Clair, 2016), to estimate the
 562 internal stress distribution within the G-layer and its consequences for macroscopic growth stress at
 563 the tree scale (Alméras *et al.*, 2009).

564



565

566 *Fig. 9. Comparative scheme of the maturation (thickening and stiffening) of the G-layer of flax and*
 567 *poplar.*

568

569 **Acknowledgements**

570 The authors are grateful to C. Assor (UMR IATE, Sup'Agro, INRAE Montpellier, France) for fruitful
 571 discussions and to D. Pellerin (ScienTec) for nanoindentation measurements. This work was
 572 performed in the framework of the project "StressInTrees" (ANR-12-BS09-0004) funded by the
 573 French National Research Agency (ANR).

574

575 **Author contributions**

576 OA participated in sample preparation, supervised and designed all the experiments and data analysis,
577 performed some of them, and contributed to writing the original draft of the paper. MC performed
578 some of the experiments and the data analysis, wrote the original draft of the paper. MR supervised
579 and performed all the experiments. FL prepared the sample and contributed fruitful discussions to the
580 data analysis. TA contributed to data analysis and to writing the original draft of the paper. GP
581 contributed to data analysis. BC contributed to data analysis, conceptualised and supervised the whole
582 project. All the authors reviewed and edited the paper and approved the final version.

583

584 **Data availability statements**

585 The datasets used and/or analysed during the current study are available from the corresponding
586 author upon reasonable request.

587

588 **References**

589 **Abedini R, Clair B, Pourtahmasi K, Laurans F, Arnould O.** 2015. Cell wall thickening in
590 developing tension wood of artificially bent poplar trees. *IAWA Journal* **36**, 44-57.

591 **Alméras T, Gril J, Yamamoto H.** 2005. Modelling anisotropic maturation strains in wood in relation
592 to fibre boundary conditions, microstructure and maturation kinetics. *Holzforschung* **59**, 347-353.

593 **Alméras T, Clair B, Gril J.** 2009. The origin of maturation stress in tension wood: using a micro-
594 mechanical model to discriminate between hypothetical mechanism. In: COST E50 final conference
595 "Systems Biology for Plant Design", Wageningen, The Netherlands, 09-11.07.2009.
596 <https://hal.archives-ouvertes.fr/hal-00797122>.

597 **Alméras T, Fournier M.** 2009. Biomechanical design and long-term stability of trees:
598 Morphological and wood traits involved in the balance between weight increase and the gravitropic
599 reaction. *Journal of Theoretical Biology* **256**, 370-381.

600 **Alméras T, Clair B.** 2016. Critical review on the mechanisms of maturation stress generation in
601 trees. *Journal of the Royal Society Interface* **13**, 20160550.

602 **Alméras T, Jullien D, Gril J.** 2018. Modelling, evaluation and biomechanical consequences of
603 growth stress profiles inside tree stems. In: Geitmann A, Gril J, eds. *Plant biomechanics: From*
604 *structure to function at multiple scale*. Berlin: Springer, 21-48.

605 **Archer RR.** 1986. Growth stresses and strains in trees. In: Timell TE, ed. *Springer Series in Wood*
606 *Science*, Berlin Heidelberg: Springer.

607 **Arnould O, Arinero R.** 2015. Towards a better understanding of wood cell wall characterisation
608 with contact resonance atomic force microscopy. *Composites: Part A* **74**, 69-76.

609 **Arnould O, Siniscalco D, Bourmaud A, Le Duigou A, Baley C.** 2017. Better insight into the nano-
610 mechanical properties of flax fibre cell walls. *Industrial Crops and Products* **97**, 224-228.

611 **Bertinetti L, Hangen UD, Eder M, Leibner P, Fratzl P, Zlotnikov I.** 2015. Characterizing
612 moisture-dependent mechanical properties of organic materials: humidity-controlled static and
613 dynamic nanoindentation of wood cell walls. *Philosophical Magazine* **95**, 1992-1998.

614 **Casdorff K, Keplinger T, Burgert I.** 2017. Nano-mechanical characterization of the wood cell wall

- 615 by AFM studies : comparison between AC- and QI mode. *Plant Methods* **13**, 60.
- 616 **Casdorff K, Keplinger T, Rüggeberg M, Burgert I.** 2018. A close-up view of the wood cell wall
617 ultrastructure and its mechanics at different cutting angles by atomic force microscopy. *Planta* doi:
618 10.1007/s00425-018-2850-9.
- 619 **Chang SS, Clair B, Ruelle J, Beauchêne J, Di Renzo F, Quignard F, Zhao GJ, Yamamoto H,**
620 **Gril J.** 2009. Mesoporosity as a new parameter in understanding of tension stress generation in trees.
621 *Journal of Experimental Botany* **60**, 3023-3030.
- 622 **Chang SS, Quignard F, Di Renzo F, Clair B.** 2012. Solvent polarity and internal stresses control
623 the swelling behavior of green wood during dehydration in organic solution. *BioResources* **7**, 2418-
624 2430.
- 625 **Chang SS, Quignard F, Alméras T, Clair B.** 2015. Mesoporosity changes from cambium to mature
626 tension wood: a new step toward the understanding of maturation stress generation in trees. *New*
627 *Phytologist* **205**, 1277-1287.
- 628 **Clair B, Arinero R, Leveque G, Ramonda M, Thibaut B.** 2003. Imaging the mechanical properties
629 of wood cell wall layers by atomic force modulation microscopy. *IAWA Journal* **24**, 223-230.
- 630 **Clair B, Gril J, Baba K, Thibaut B, Sugiyama J.** 2005a. Precaution for the structural analysis of
631 the gelatinous layer in tension wood. *IAWA Journal* **26**, 189-195.
- 632 **Clair B, Thibaut B, Sugiyama J.** 2005b. On the detachment of gelatinous layer in tension wood
633 fibre. *Journal of Wood Science* **51**, 218-221.
- 634 **Clair B, Gril J, Di Renzo F, Yamamoto H, Quignard F.** 2008. Characterization of a gel in the cell
635 wall to elucidate the paradoxical shrinkage of tension wood. *Biomacromolecules* **9**, 494-498.
- 636 **Clair B, Alméras T, Pilate G, Jullien D, Sugiyama J, Riekel C.** 2011. Maturation stress generation
637 in poplar tension wood studied by synchrotron radiation micro-diffraction. *Plant Physiology* **155**,
638 562-570.
- 639 **Coste R, Pernes M, Tetard L, Molinari M, Chabbert B.** 2020. Effect of the interplay of
640 composition and environmental humidity on the nanomechanical properties of hemp fibers. *ACS*
641 *Sustainable Chemistry and Engineering* **8**, 6381-6390.
- 642 **Coste R, Soliman M, Bercu NB, Potiron S, Lasri K, Aguié-Béghin V, Tetard L, Chabbert B,**
643 **Molinari M.** 2021. Unveiling the impact of embedding resins on the physicochemical traits of wood
644 cell walls with subcellular functional probing. *Composites Science and Technology* **201**, 108485.
- 645 **Côté WA, Day AC, Timell TE.** 1969. A contribution to the ultrastructure of tension wood fibers.
646 *Wood Science and Technology* **3**, 257-271.
- 647 **Dadswell HE, Wardrop AB.** 1955. The structure and properties of tension wood. *Holzforschung* **9**,
648 97-104.
- 649 **Decou R, Labrousse P, Béré E, Fleurat-Lessard P, Krausz P.** 2020. Structural features in tension
650 wood and distribution of wall polymers in the G-layer of in vitro grown poplars. *Protoplasma* **257**,
651 13-29.
- 652 **Derjaguin BV, Muller VM, Toporov, YP.** 1975. Effect of contact deformations on the adhesion of
653 particles. *Journal of Colloid and Interface Science* **53**, 314-326.
- 654 **Eder M, Arnould O, Dunlop JWC, Hornatowska J, Salmén L.** 2013. Experimental
655 micromechanical characterisation of wood cell walls. *Wood Science and Technology* **47**, 163-182.
- 656 **Fahlén J, Salmén L.** 2002. On the lamellar structure of the tracheid cell wall. *Plant Biology* **4**, 339-
657 345.
- 658 **Fang CH, Clair B, Gril J, Alméras T.** 2007. Transverse shrinkage in G-fibers as a function of cell

- 659 wall layering and growth strain. *Wood Science and Technology* **41**, 659-671.
- 660 **Fang CH, Clair B, Gril J, Liu S.** 2008. Growth stresses are highly controlled by the amount of G-
661 layer in poplar tension wood. *IAWA Journal* **29**, 237-246.
- 662 **Fournier M, Alméras T, Clair B, Gril J.** 2014. Biomechanical action and biological functions. In:
663 Gardiner B, Barnett J, Saranpää P, Gril J, eds. *The biology of reaction wood*. Berlin: Springer, Berlin,
664 139-169.
- 665 **Ghislain B, Nicolini EA, Romain R, Ruelle J, Yoshinaga A, Alford MH, Clair B.** 2016.
666 Multilayered structure of tension wood cell walls in *Salicaceae sensu lato* and its taxonomic
667 significance. *Botanical Journal of the Linnean Society* **182**, 744-756.
- 668 **Ghislain B, Clair B.** 2017. Diversity in organisation and lignification of tension wood fibre walls –
669 a review. *IAWA Journal* **38**, 245-265.
- 670 **Gindl W, Gupta HS, Grünwald C.** 2002. Lignification of spruce tracheid secondary cell walls
671 related to longitudinal hardness and modulus of elasticity using nano-indentation. *Canadian Journal*
672 *of Botany* **80**, 1029-1033.
- 673 **Gorshkova TA, Morvan C.** 2006. Secondary cell-wall assembly in flax phloem fibres: role of
674 galactans. *Planta* **223**, 149-158.
- 675 **Gorshkova TA, Gurjanov OP, Mikshina PV, Ibragimova NN, Mokshina NE, Salnikov VV,**
676 **Ageeva MV, Amenitskii SI, Chernova TE, Chemikosova SB.** 2010. Specific type of secondary
677 cell wall formed by plant fibers. *Russian Journal of Plant Physiology* **57**, 328-341.
- 678 **Gorshkova TA, Mokshina N, Chernova T, Ibragimova N, Salnikov V, Mikshina P, Tryfona T,**
679 **Banasiak A, Immerzeel P, Dupree P, Mellerowicz EJ.** 2015. Aspen tension wood fibers contain β -
680 (1 \rightarrow 4)-galactans and acidic arabinogalactans retained by cellulose microfibrils in gelatinous walls.
681 *Plant Physiology* **169**, 2048-2063.
- 682 **Goswami L, Dunlop JWC, Jungnikl K, Eder M, Gierlinger N, Coutand C, Jeronimidis G, Fratzl**
683 **P, Burgert I.** 2008. Stress generation in the tension wood of poplar is based on the lateral swelling
684 power of the G-layer. *The Plant Journal* **56**, 531-538.
- 685 **Goudenhooff C, Siniscalco D, Arnould O, Bourmaud A, Sire O, Gorshkova T, Baley C.** 2018.
686 Investigation of the mechanical properties of flax cell walls during plant development: the relation
687 between performance and cell wall structure. *Fibers* **6** doi: 10.3390/fib6010006.
- 688 **Grozdits GA, Ifju G.** 1969. Development of tensile strength and related properties in differentiating
689 coniferous xylem. *Wood Science* **1**, 137-147.
- 690 **Guedes FTP, Laurans F, Quemener B, Assor C, Lainé-Prade V, Boizot N, Vigouroux J, Lesage-**
691 **Descauses MC, Lepié JC, Déjardin A, Pilate G.** 2017. Non-cellulosic polysaccharide distribution
692 during G-layer formation in poplar tension wood fibers: abundance of rhamnogalacturonan I and
693 arabinogalactan proteins but no evidence of xyloglucan. *Planta* **246**, 857-878.
- 694 **Huang Y, Fei B, Wei P, Zhao C.** 2016. Mechanical properties of bamboo fiber cell walls during the
695 culm development by nanoindentation. *Industrial Crops and Products* **92**, 102-108.
- 696 **Hermanowicz P, Sarna M, Burda K, Gabrys H.** 2014. AtomicJ: An open source software for
697 analysis of force curves. *Review of Scientific Instruments* **85**, 063703.
- 698 **Hock CW.** 1942. Microscopic structure of flax and related bast fibres. *Journal of Research of the*
699 *National Bureau of Standards* **29**, 41-50.
- 700 **Jäger A, Bader T, Hofstetter K, Eberhardsteiner J.** 2011. The relation between indentation
701 modulus, microfibril angle, and elastic properties of wood cell walls. *Composites Part A: Applied*
702 *Science and Manufacturing* **42**, 677-685.
- 703 **Jakes JE, Frihart CR, Beecher JF, Moon RJ, Stone DS.** 2008. Experimental method to account

704 for structural compliance in nanoindentation measurements. *Journal of Materials Research* **23**, 1113-
705 1127.

706 **Jakes JE, Frihart CR, Beecher JF, Moon RJ, Resto P, Melgarejo Z, Suárez OM, Baumgart H,**
707 **Elmustafa AA, Stone DS.** 2009. Nanoindentation near the edge. *Journal of Materials Research* **24**,
708 1016-1031.

709 **Johnson KL.** 1987. *Contact mechanics*. Cambridge University Press.

710 **Johnson KL, Greenwood JA.** 1997. An adhesion map for the contact of elastic spheres. *Journal of*
711 *Colloid Interface Science* **192**, 326-333.

712 **Konnerth J, Harper D, Lee SH, Rials TG, Gindl W.** 2008. Adhesive penetration of wood cell walls
713 investigated by scanning thermal microscopy (SThM). *Holzforschung* **62**, 91-98.

714 **Kozlova L, Petrova A, Ananchenko B, Gorshkova T.** 2019. Assessment of primary cell wall
715 nanomechanical properties in internal cells of non-fixed maize roots. *Plants* **8**, 172.

716 **Liang R, Zhu YH, Yang X, Gao JS, Zhang YL, Cai LP.** 2020. Study on the ultrastructure and
717 properties of gelatinous layer in poplar. *Journal of Materials Science* **56**, 415–427.

718 **Luo L, Zhu Y, JGui J, Yin T, Luo W, Liu J, Li L.** 2021. A comparative analysis of transcription
719 networks active in juvenile and mature wood in *Populus*. *Frontiers in Plant Science* **12**, 675075.

720 **Mellerowicz EJ, Gorshkova TA.** 2012. Tensional stress generation in gelatinous fibres: a review
721 and possible mechanism based on cell-wall structure and composition. *Journal of Experimental*
722 *Botany* **63**, 551-565.

723 **Meng Y, Xia Y, Young TM, Cai Z, Wang S.** 2015. Viscoelasticity of wood cell walls with different
724 moisture content as measured by nanoindentation. *RSC Advances* **5**, 47538.

725 **Moullia B, Coutand C, Lenne C.** 2006. Posture control and skeletal mechanical acclimation in
726 terrestrial plants: implications for mechanical modeling of plant architecture. *American Journal of*
727 *Botany* **93**, 1477-1489.

728 **Muraille L, Aguié-Béghin V, Chabbert B, Molinari M.** 2017. Bioinspired lignocellulosic films to
729 understand the mechanical properties of lignified plant cell walls at nanoscale. *Scientific Reports* **7**,
730 44065.

731 **Nair SS, Wang S, Hurley DC.** 2010. Nanoscale characterization of natural fibers and their
732 composites using contact-resonance force microscopy. *Composites: Part A* **41**, 624-631.

733 **Niklas KJ.** 1992. *Plant biomechanics. An engineering approach to plant form and function*. Chicago:
734 University of Chicago Press.

735 **Normand AC, Charrier AM, Arnould O, Lereu AL.** 2021. Influence of force volume indentation
736 parameters and processing method in wood cell walls nanomechanical studies. *Scientific Reports* **11**,
737 5739.

738 **Okumura S, Harada H, Saiki H.** 1977. Thickness variation of the G-layer along a mature and a
739 differentiating tension wood fiber in *Populus euramericana*. *Wood Science and Technology* **11**, 23-
740 32.

741 **Okuyama T, Yamamoto H, Yoshida M, Hattori Y, Archer RR.** 1994. Growth stresses in tension
742 wood: role of microfibrils and lignification. *Annales des Sciences Forestières* **51**, 291-300.

743 **Onaka F.** 1949. Studies on compression and tension wood. *Wood Research* **1**, 1-88.

744 **Özparpucu M, Rüggeberg M, Gierlinger N, Cesarino I, Vanholme R, Boerjan W, Burgert I.**
745 2017. Unravelling the impact of lignin on cell wall mechanics: a comprehensive study on young
746 poplar trees downregulated for CINNAMYL ALCOHOL DEHYDROGENASE (CAD). *The Plant*
747 *Journal* **91**, 480-490.

- 748 **Özparpucu M, Gierlinger N, Cesarino I, Burgert I, Boerjan W, Rüggeberg M.** 2019. Significant
749 influence of lignin on axial elastic modulus of poplar wood at low microfibril angles under wet
750 conditions. *Journal of Experimental Botany* **70**, 4039-4047.
- 751 **Peaucelle A.** 2014. AFM-based mapping of the elastic properties of cell walls: at tissue, cellular, and
752 subcellular resolutions. *Journal of Visualized Experiments* **89**, e51317.
- 753 **Petrova A, Kozlova L, Gorshkov O, Nazipova A, Ageeva M, Gorshkova T.** 2021. Cell wall layer
754 induced in xylem fibers of flax upon gravistimulation is similar to constitutively formed cell walls of
755 bast fibers. *Frontiers in Plant Science* **12**, 660375.
- 756 **Pilate P, Déjardin A, Laurans F, Leplé JC.** 2004. Tension wood as a model for functional genomics
757 of wood formation. *New Phytologist* **164**, 63-72.
- 758 **Pot G, Coutand C, Le Cam JB, Toussaint E.** 2013a. Experimental study of the mechanical
759 behaviour of thin slices of maturing green poplar wood using cyclic tensile tests. *Wood Science and*
760 *Technology* **47**, 7-25.
- 761 **Pot G, Toussaint E, Coutand C, Le Cam JB.** 2013b. Experimental study of the viscoelastic
762 properties of green poplar wood during maturation. *Journal of Materials Science* **48**, 6065-6073.
- 763 **Pot G, Coutand C, Toussaint E, Le Cam JB, Saudreau M.** 2014. A model to simulate the
764 gravitropic response and internal stresses in trees, considering the progressive maturation of wood.
765 *Trees* doi: 10.1007/s00468-014-1033-y
- 766 **Richardson KC, Jarett L, Finke EH.** 1960. Embedding in epoxy resins for ultrathin sectioning in
767 electron microscopy. *Stain Technology* **35**, 313-323.
- 768 **Scurfield G.** 1973. Reaction wood: its structure and function. *Science* **179**, 647-655.
- 769 **Sell J, Zimmermann T.** 1998. The fine structure of the cell wall of hardwoods on transverse-fracture
770 surfaces. *European Journal of Wood and Wood Products* **56**, 365-366.
- 771 **Sudharshan Phani P, Oliver WC.** 2019. A critical assessment of the effect of indentation spacing
772 on the measurement of hardness and modulus using instrumented indentation testing. *Materials and*
773 *Design* **164**, 107563.
- 774 **Thibaut B, Gril J, Fournier M.** 2001. Mechanics of wood and trees: some new highlights for an old
775 story. *Comptes Rendus de l'Académie des Sciences – Series IIB* **329**, 701-716.
- 776 **Wagner L, Bader TK, De Borst K.** 2014. Nanoindentation of wood cell walls: effects of sample
777 preparation and indentation protocol. *Journal of Materials Science* **49**, 94-102.
- 778 **Wang X, Ren H, Zhang B, Fei B, Burgert I.** 2012. Cell wall structure and formation of maturing
779 fibres of moso bamboo (*Phyllostachys pubescens*) increase buckling resistance. *Journal of the Royal*
780 *Society Interface* **9**, 988-996.
- 781 **Xu D, Liechti KM, Ravi-Chandar K.** 2007. On the modified Tabor parameter for the JKR–DMT
782 transition in the presence of a liquid meniscus. *Journal of Colloid and Interface Science* **315**, 772-
783 785.
- 784 **Yamamoto H.** 1998. Generation mechanism of growth stresses in wood cell walls: roles of lignin
785 deposition and cellulose microfibril during cell wall maturation. *Wood Science and Technology* **32**,
786 171–182.
- 787 **Yoshinaga A, Kusumoto H, Laurans F, Pilate G, Takabe K.** 2012. Lignification in poplar tension
788 wood lignified cell wall layers. *Tree Physiology* **32**, 1129-1136.
- 789 **Zhang SY, Fei BH, Wang CG.** 2016. Effects of chemical extraction treatments on nano-scale
790 mechanical properties of the wood cell wall. *BioResources* **11**, 7365-7376.